

# Real-time Event Recognition of Long-distance Distributed Vibration Sensing with Knowledge Distillation and Hardware Acceleration

Zhongyao Luo, Hao Wu, Zhao Ge, and Ming Tang, *Senior Member, IEEE*,

**Abstract**—Distributed optical fiber vibration sensing (DVS) technology based on phase-sensitive optical time-domain reflectometry is widely used for safety monitoring and intrusion event surveillance in wide-ranging fields. Existing methods rely on deep learning models for event recognition but struggle with real-time processing of large data volumes in long-distance applications. To address these challenges, we use a four-layer convolutional neural network (CNN). The application of knowledge distillation with ResNet as the teacher model improves the generalization ability of the four-layer CNN, increasing the accuracy from 83.41% to 95.39% on data from untrained environments. The model is implemented on a field programmable gate array (FPGA) using a novel design that replaces multiplication with binary shift operations and quantizes model weights accordingly, allowing for high parallelism and low latency. An inference time of 0.083 ms is achieved for a spatial-temporal sample with a 12.5 m fiber length and 0.256 s time frame. This implies the system can process signals over a fiber length of approximately 38.55 km in real time, which is more than twice the capability of a GPU of Nvidia GTX 4090. The proposed method greatly improves the efficiency of vibration pattern recognition, thus promoting the application of DVS as smart sensing system in various areas. The data and code is available at <https://github.com/HUST-IOF/Efficient-DVS>.

**Index Terms**—distributed vibration sensing, convolutional neural network, hardware acceleration, real-time system, fiber-optic IoT

## I. INTRODUCTION

**D**ISTRIBUTED optical fiber vibration sensing (DVS) technology is based on phase-sensitive optical time-domain reflectometry (phi-OTDR) system, and uses optical fibers as the sensing element. It is capable of providing dense and continuous wide-range measurement of vibration from surrounding environment and recognize various intrusion events based the sampled data. This technology has been applied as smart sensing system in various areas in recent years, including railway safety monitor [1], [2], perimeter security [3], [4], pipeline monitor [5], [6], and smart city [7]. As shown in Fig. 1, the phi-OTDR system captures the backscattering

This work was supported in part by the National Key Research and Development Program of China under Grant 2021YFB2800902; in part by the National Natural Science Foundation of China under Grant 62225110; and in part by the innovation Fund of WNLO. (Corresponding author: Hao Wu).

The authors are with the Wuhan National Laboratory for Optoelectronics, Next Generation Internet Access National Engineering Laboratory, and Hubei Optics Valley Laboratory, School of Optical and Electronic Information, Huazhong University of Science and Technology, Wuhan 430074, China (email: zluo@hust.edu.cn, wuhaoboom@hust.edu.cn, d202280977@hust.edu.cn, tangming@mail.hust.edu.cn)

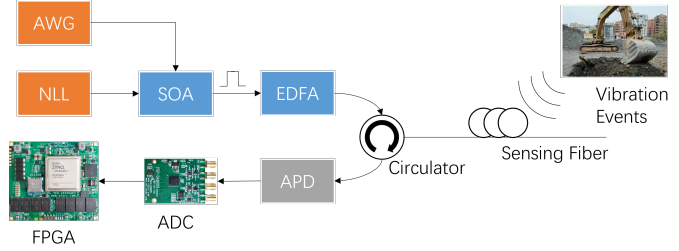


Fig. 1. Schematic of DVS system. NLL: narrow linewidth laser, SOA: semiconductor optical amplifier, AWG: arbitrary waveform generator, EDFA: erbium-doped fiber amplifier, FUT: fiber under test, APD: avalanche photodiode, DAQ: data acquisition card.

Rayleigh light across the fiber. The collected Rayleigh light trace, whose phase can be affected by external vibration, provides valuable information about the vibration events. Signal processing algorithms are able to extract information from vibration traces. However, the recognition accuracy of vibration events is often limited by the variability of signals caused by complex and changing environments, as well as the diverse types of intrusion events encountered in practical applications. To improve the recognition performance, conventional methods typically involve hand-crafted algorithms for data preparation and feature extraction, followed by the use of classic machine learning algorithms for recognition [8]–[13]. However, this kind of approaches can be time-consuming in both development and deployment. Designing feature extraction algorithms requires researchers to possess knowledge of signal processing algorithms and the specific application context. As a result, the resulting algorithms can be complex, time-consuming, and may not capture the most important features accurately.

To address these challenges, deep learning models (DLMs) have been introduced to the field. Initially, DLMs were introduced for pattern recognition based on extracted features [9]. With the development of more sophisticated and computationally powerful DLMs, they are capable of automatically extracting important features from noisy data and simultaneously handling feature extraction and pattern recognition tasks. The introduction of complex DLMs brings about improved performance and reduces the design workload. Consequently, they have received more attention in recent years. Table I shows several typical methods of this type of application, where *GAF* represents gramian angular field, *S*–*T* denotes space-time, and *F*–*T* is frequency-time.

TABLE I  
PREVIOUS WORK ON DLM-BASED DVS ALGORITHMS AND OUR WORK

Model	Input Form	Parameter Number	Accuracy (%)	Pub. Year
VGG16	GAF Figure	138M	97.67	2020 [3]
Yolov3	S-T Image	45.5M	-	2021 [14]
Yolo-A30	S-T Image	65M	99.2	2022 [2]
Yolo	S-T Image	61M	96.1	2022 [15]
MTL	S-T Image	1.13M	99.46	2023 [7]
Swin-T	GAF Figure	28M	92.44	2023 [6]
Resnet-152	F-T Image	60M	96.67	2023 [16]
CNN-4 (This work)	S-T Image	30K	95.39	-

However, the utilization of high-capacity DLMs has resulted in increased computation resource requirements. Moreover, when using the DVS system to monitor optical fibers, it is important to note that the volume of captured data directly relates to the length of the fiber. Due to the limited available computation resources in real-world applications, achieving real-time recognition is only possible over short-distance fibers [17]. To improve the computational efficiency of the DVS system, there are typically three solutions. The first is data selection or down-sampling, which involves using prior knowledge and data analysis to identify and retain valuable signal sections or sample points [2], [7]. This approach aims to reduce the input data volume through hand-crafted algorithms, though it may result in false negatives. The second solution is model compression, which seeks to lower computational complexity and resource demands. However, existing solutions use models with a parameter number no lower than millions to ensure performance and generalizability [7]. So, there is still potential for further improvement to create smaller and more efficient models. The third solution is the use of high-performance hardware, such as graphics processing units (GPUs) and cloud computing. While this approach can significantly increase computational power, it is often expensive and demands high power consumption, as well as a reliable communication system to handle the large volume of sample data.

This paper proposes to improve the signal processing capability of the DVS system through knowledge distillation and hardware acceleration. We propose to use a shallow convolutional neural network (CNN), instead of DLMs, to reduce model complexity and computation resource requirements. Moreover, we identify the generalizability limitation of low-capacity models and propose to use the knowledge distillation technique as a solution. To further improve the throughput of the data processing system, we design an efficient hardware acceleration scheme based on field programmable gate array (FPGA). Additionally, we have integrated an Analog-to-Digital Converter (ADC) with the FPGA to minimize latency during data transfer, as depicted in Fig. 1. The proposed scheme utilizes FPGA's flexibility to achieve full optimization of the model. It involves replacing multiplication operations in the model inference with shift operations, as the later ones can be implemented without digital signal processing (DSP) resources. This design is only limited by the logic resources, instead of DSP resources which is more limited [18], on the chip, allows for higher parallelism and thus faster calculation. This architecture is referred as the shift-add structure in the rest of the paper. Additionally, we propose to quantize the model weights into integers that indicate the

number of binary shift operations. The quantization technique is referred as shift parameter quantization in the rest of the paper. Through this approach, we can achieve real-time processing of a large amount of captured data from the DVS system on a mainstream industrial FPGA.

In a word, the contribution of this work can be listed as follows:

- We propose a novel scheme for designing and implementing real-time DVS algorithms and evaluate it using real-world DVS datasets. The results demonstrate comparable performance and generalizability to deep learning models, while achieving real-time recognition over long-distance fibers.
- Shallow CNN models, coupled with knowledge distillation, are used to develop a lightweight model that offers high performance and generalizability. This approach effectively addresses the throughput limitation brought by the high computational complexity of existing algorithms.
- A novel hardware acceleration scheme targeted for shallow CNN is developed, leveraging shift-add structures and shift parameter quantization to achieve higher efficiency.

## II. METHOD

### A. Knowledge Distillation based on logits

It is generally believed that large models, that is, models with more complex and efficient structural design and huge number of parameters, tend to be able to extract higher-level features, so that it can achieve better results in various tasks. In other words, large models often have better generalizability, and can better handle signals with various noise. On the other hand, the model inference process can be considered as finishing the specified task based on the 'knowledge' contained in model structure and its parameters. The idea of knowledge distillation is to extract the knowledge from large models (teacher models), and transfer the knowledge to small models (student model), so that the performance and generalizability of the later one can be improved. In the knowledge distillation method based on logits [19], the output prediction distribution of the model is considered to contain valuable knowledge. This distribution represents the probabilities of classifying the input sample into each class. The distribution can be obtained through introducing a temperature parameter  $T$  to the softmax function at output layer. The function can be expressed as:

$$\text{Softmax}(\mathbf{x}/T)_i = \frac{e^{x_i/T}}{\sum_j e^{x_j/T}} \quad (1)$$

where  $\mathbf{x} = [x_1, x_2, \dots, x_n]$  is the input vector, which is the output of the network in this case. The knowledge is then transferred by guiding the student model to imitate the behavior of the teacher model. The process is to minimizing a loss function that measures the difference between the outputs of the teacher network and the student network, and also the difference between the outputs of the student network and the correct results, as shown in Fig. 2. The process can be seen as minimizing the difference between the outputs of the student network and the correct results. It can be achieved through

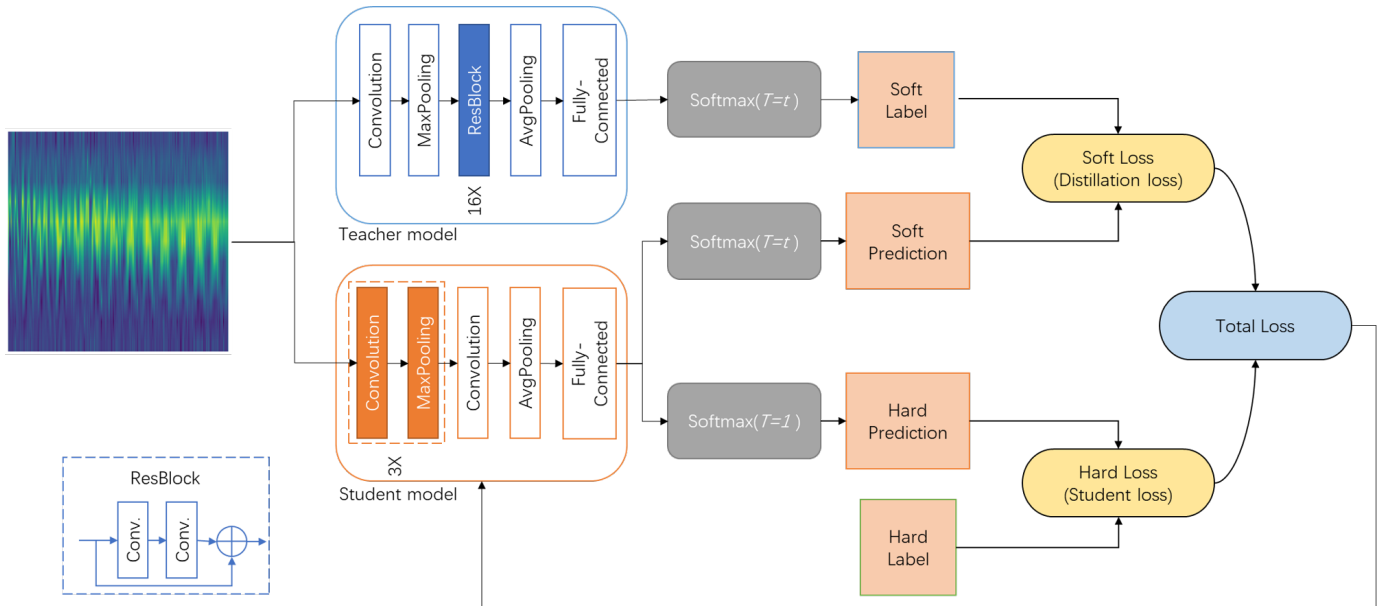


Fig. 2. Schematic of KD process.

minimizing a loss function that measures the difference between the outputs of the teacher network and the student network. The loss function usually consists of a standard classification loss, like cross-entropy, and a distillation loss that measures the difference between the softened probabilities generated by the teacher and student networks. Formally, the loss function  $\mathcal{L}$  can be expressed as:

$$\mathcal{L} = \alpha \cdot \text{CE}(\mathbf{y}_s, \mathbf{y}_{\text{true}}) + (1 - \alpha) \cdot \text{KL}(\text{Softmax}(\mathbf{y}_t/T), \text{Softmax}(\mathbf{y}_s/T)) \quad (2)$$

where  $\text{CE}$  denotes the cross-entropy loss,  $\text{KL}$  represents the Kullback-Leibler divergence,  $\mathbf{y}_{\text{true}}$  is the true label,  $\alpha$  represents weight between two kind of losses,  $\mathbf{y}_t$  and  $\mathbf{y}_s$  denote the outputs of the teacher and student networks respectively. Through this optimization process, knowledge distillation enables the creation of compact yet powerful neural networks capable of retaining the performance of their larger counterparts.

### B. FPGA-Based Hardware Acceleration

1) *Parallel Architecture*: The main problem of implementing CNN on FPGA is the storage of intermediate data generated during the calculation process and the parameters of the model [20]. There are two typical solutions to the problem. One option is to use external memory to expand the storage capacity [18], [21]–[23]. This type of design usually combines on-chip storage and external storage to form a cache system. The on-chip computing unit and memory access pattern is designed in accordance with the bandwidth limitation of the cache system. The model is divided into multiple computing tasks suitable for the computing unit. As the tasks are completed in sequence, the calculation of the entire model is also completed. Another option is to compress the model and store all intermediate data and parameters on-chip [18], [20]. Such design typically adopts a pipeline structure, implementing the

model as multiple parallel modules to improve the throughput of the design. In this paper, in order to achieve faster inference efficiency, the later one is adopted. Each layer of the model is implemented as a separate module as shown in Fig. 3.

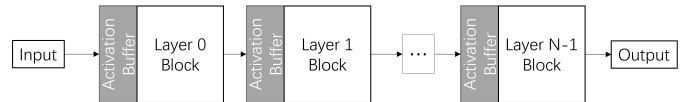


Fig. 3. Schematic of pipelined structure.

2) *Activation Buffering*: The activation buffer, as shown in Fig. 3, stores intermediate data from the preceding layer. A typical convolution and max pooling layer can be expressed as follows:

$$O_{conv}[m, x, y] = \sum_{n=0}^{N-1} \sum_{p=0}^{P-1} \sum_{q=0}^{Q-1} I[n, x + p, y + q] * K[m, n, p, q] + B[m] \quad (3)$$

$$O_{max}[n, x, y] = \max\{I[n, x : x + P, y : y + Q]\} \quad (4)$$

Here, the symbols  $O$ ,  $I$ ,  $M$ ,  $N$ ,  $P$ ,  $Q$ ,  $K$ , and  $B$  represent the following components:  $O$  denotes the output feature map,  $I$  represents the input feature map,  $M$  corresponds to the number of output channels,  $N$  denotes the number of input channels,  $P$  represents the kernel height,  $Q$  represents the kernel width,  $K$  symbolizes the convolution kernel, and  $B$  signifies the bias term.

Obviously, both convolution layers and pooling layers only require the input feature map data within the selected window. Assume the input to be a spatial-temporal figure, where rows represent discrete times and columns represent positions. The data is streamed in row-major order. Then the activation buffer only needs to store  $P$  rows from the input feature map

during the computation process. Thus, the buffer mechanism is designed as shown in Fig. 4.

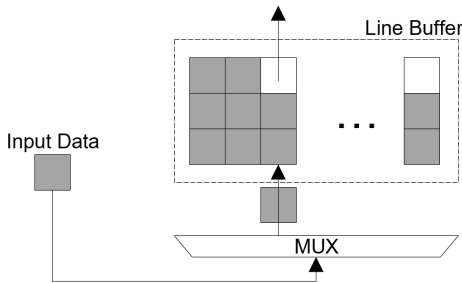


Fig. 4. Line buffer structure.

When new data is inputted, the corresponding column shifts the existing data up by one unit, and the new data is filled into the bottom unit. This design allows the buffer to store just  $P-1$  rows and  $Q$  data from the last row to start the convolution operation. Thus, the design only requires  $P$  rows of storage capacity. Moreover, reading new data and calculation can be performed in parallel to achieve lower latency. The convolution layer only needs to buffer  $(P-1-S) \times W + Q$  data for each channel instead of the complete input feature map to start operation, where  $W$  and  $S$  denote the width of input feature map and the stride respectively. Thank you for the clarification. I apologize for the misunderstanding. In the case of a convolution layer, it only needs to buffer  $(P-1-S) \times W + Q$  data for each channel, rather than the entire input feature map, in order to commence the operation. Here,  $W$  represents the width of the input feature map, and  $S$  represents the stride.

3) *Shift-Add Structure*: The main operation of convolutional neural networks is multiplication and accumulation (MAC). Digital signal processing (DSP) block is required to implement MAC units on FPGA. The limited number of DSP blocks restricts the number of MAC units that can be implemented on-chip. As a result, the throughput of the design is restricted. To avoid this restriction, it is proposed to use the shift and accumulation units that do not require DSP resources for implementation to replace the MAC units, as shown in Fig. 5. Digital values can be represented as a sum of powers of 2, as illustrated in Equation 5 with exponents denoted as  $s_0, s_1, \dots, s_k$ . Multiplication with power of two is essentially performing shift operations on multiplier. This allows a MAC operations to be losslessly replaced by a series of shift and accumulation operations, as shown in Equation 6.

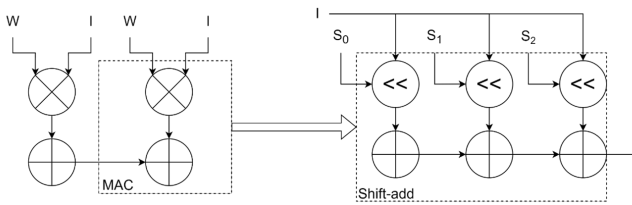


Fig. 5. Shift-add and MAC structure.

$$W = 2^{s_0} + 2^{s_1} + \dots + 2^{s_k} \quad (5)$$

$$\begin{aligned} I \cdot W &= I \cdot (2^{s_0} + 2^{s_1} + \dots + 2^{s_k}) \\ &= I \ll s_0 + I \ll s_1 + \dots + I \ll s_k \end{aligned} \quad (6)$$

4) *Shift Parameter Quantization*: After converting all the MAC operations to shift and accumulation operations, the powers of two in the above equation 5 and 6 can be seen as separate parameters representing number of shift and accumulation operations, which are referred as shift parameters in this paper. To reduce the latency and demand for storage space of the design, a magnitude-based post-training pruning strategy is employed here to reduce the number of the shift parameters [24]. It is to assume that the smaller parameters have less impact on the final output, i.e., less significant. Based on this assumption, the smaller parameters can be discarded without severe influence on the final performance of the model. The complete quantization process is briefly described in detail with pseudo code shown in Algorithm 1.

---

#### Algorithm 1 Shift Parameter Quantization

---

```

1: Input
2:   Params      matrix of parameters
3:   N          Number of parameters remained
4: Output
5:   Shifts     Quantized parameters
6:   Signs      Sign of parameters
7:
8:   Signs  $\leftarrow$  SIGN(Params)
9:   [rows, cols]  $\leftarrow$  SHAPE(Params)
10:  for  $i = 1$  to  $rows - 1$  do
11:    for  $j = 1$  to  $cols - 1$  do
12:      BitPositions  $\leftarrow$  ZEROS( $N$ )
13:      count  $\leftarrow 0$ 
14:       $P_{binary} \leftarrow$  BINARY( $AbsParams[i][j]$ )
15:      for  $i \leftarrow 0$  to LEN( $P_{binary}$ ) - 1 do
16:        if count  $< N$  then
17:          if  $P_{binary}[i] = 1$  then
18:            BitPositions[count]  $\leftarrow i + 1$ 
19:            count  $\leftarrow count + 1$ 
20:          else
21:            BitPositions[count]  $\leftarrow$  None
22:          end if
23:        end if
24:      end for
25:      Shifts[i][j][:]  $\leftarrow$  BitPositions
26:    end for
27:  end for

```

---

Conventional quantization methods typically involve mapping weights to a limited integer range [25]. The output data of the quantized layer requires to be mapped back to the original value range before it can be used as input of the subsequent layers. The proposed method does not require such operations. Thus, the hardware design does not need any DSP block to implement the floating-point multipliers. As a result, the design can avoid potential throughput limitations related to DSP resources limitation.

5) *Encoding*: After quantization, the next step is to encode the parameters for storage. In order to further compress the storage space required for parameters, offset binary encoding is used [26]. The offset binary encoding scheme introduces an offset to reposition the data within an optimal range before performing binary encoding. In this scheme, the data is moved towards zero. In the encoding process, we first extract and save the sign information of the parameters. Then, we perform quantization on the absolute value of the parameters. The bias is chosen based on the smallest non-zero number to ensure that it is moved to zero. The parameters that are outside the data range of the majority of parameters are rounded to the nearest number. The pseudo code of the process is shown in Algorithm 2.

---

**Algorithm 2** Biased Binary Encoding

---

```

1: Input
2:   Params      matrix of parameters
3:   N          Number of bits used for encoding
4: Output
5:   Encoded    Encoded parameters
6:   Bias       Bias for the encoding
7:   Signs      Sign of parameters
8:
9: MinValue  $\leftarrow \text{MIN}(\text{Params})$ 
10: Bias  $\leftarrow -\text{MinValue}$ 
11: MaxRange  $\leftarrow 2^N - 1$ 
12: Signs  $\leftarrow \text{SIGN}(\text{Params})$ 
13: AbsParams  $\leftarrow \text{ABS}(\text{Params})$ 
14: [rows,cols]  $\leftarrow \text{SHAPE}(\text{Params})$ 
15: for i = 1 to rows - 1 do
16:   for j = 1 to cols - 1 do
17:     Pbiased  $\leftarrow \text{AbsParams}[\text{i}][\text{j}] + \text{bias}$ 
18:     if Pbiased > MaxRange then
19:       Pbiased  $\leftarrow \text{MaxRange}$ 
20:     end if
21:     Pencoded  $\leftarrow \text{BINARY}(\text{Pbiased})$ 
22:     Encoded[\i][\j]  $\leftarrow \text{Pencoded}$ 
23:   end for
24: end for

```

---

### III. EXPERIMENT

The proposed scheme is evaluated using a real-world dataset captured by a DVS system, as illustrated in Fig. 1. The system capture a trace of Rayleigh back scattering light every 1 ms, with a spatial interval of 1.25 m. The samples stored as a 2-dimensional matrix with a size of 256 by 11, represent spatial-temporal figures, capturing a segment of the fiber with a length of 12.5 m and a time frame of 0.256 s. A 30 km long fiber was utilized, with a section of 50 m buried under 0.5 m of composite material composed of soil, sand, and stones in random ratios. The composition of the material has a significant impact on the vibration signal detected by the fiber, making it an effective means to explore the influence of environmental complexity. The dataset comprises two parts, collected from different locations at different time with varying

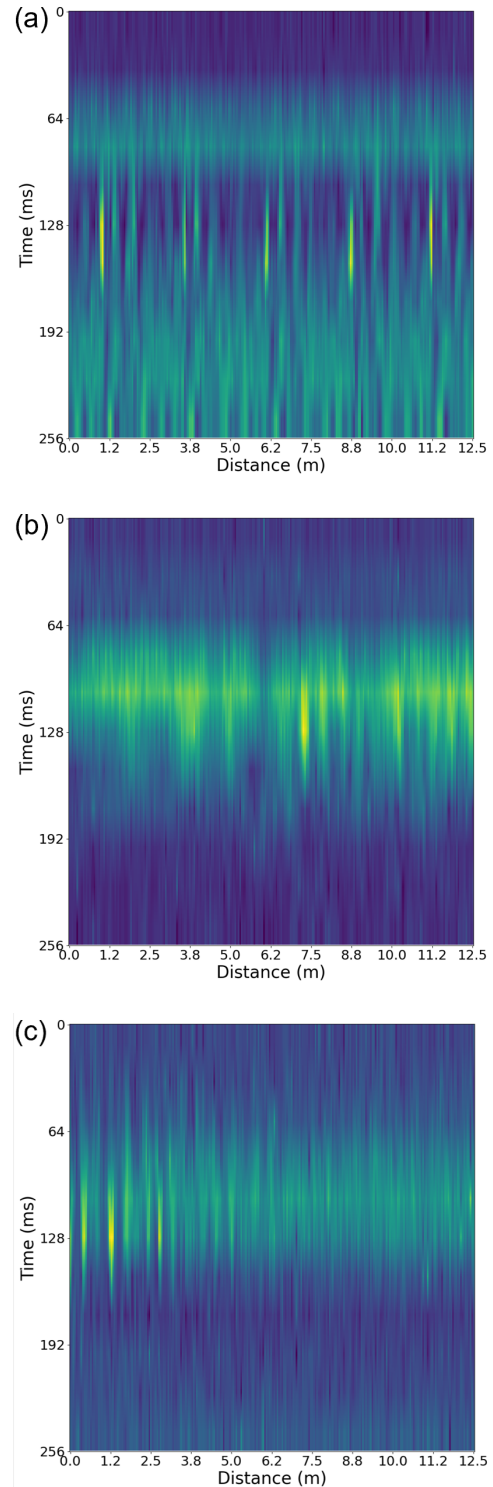


Fig. 6. Visualization of typical data samples. (a) Air Pick. (b) Excavator. (c) Hammer.

material compositions, simulating the installation of the system in different environments for the same application. Specific details regarding the composition of the datasets are provided in Table II. Typical data are shown in Fig. 6.

TABLE II  
CLASS LABEL AND DISTRIBUTION OF SAMPLES OF THE DATASETS

Class	Dataset 1	Dataset 2
Hammer	3332	268
Air Pick	3558	330
Excavator	3359	277

### A. Performance evaluation

To evaluate and demonstrate the effectiveness of the proposed scheme, we employ a 5-fold cross-validation strategy on Dataset 1. This strategy involves dividing the dataset into five equally-sized subsets or folds. The division of folds remains consistent throughout the subsequent evaluations to ensure fair comparison of results. During each iteration of the cross-validation process, the model is trained on four folds while the remaining fold is held out for validation. This process is repeated five times, with each fold serving as the validation set once. The Dataset 2 is used as test set to verify the generalizability of the model. By averaging the performance of the five runs, we obtain the final validation and test result. Adam optimizer is used for training. Learning rate is set to 0.001, and it is halved when the training loss does not decrease within five epochs. The training setting is also kept consistent for the subsequent evaluations.

TABLE III  
PARAMETERS OF THE CNN MODEL

Layers	Kernel Size	Stride	Padding	Ouput Channels
Conv 1	3*3	1	1	8
MaxPool 1	2*2	2	0	8
Conv 2	3*3	1	1	16
MaxPool 2	2*2	2	0	16
Conv 3	3*3	1	1	32
AvgPool 1	2*2	2	0	32
Conv 4	3*3	1	1	64
flatten	-	-	-	2048
FC 1	-	-	-	3

To evaluate and demonstrate the performance of the lightweight model, a 4-layer CNN with a structure outlined in Table III is utilized. The model consists of four layers and has a total of 30,771 parameters. In terms of computational cost, it requires 2,282,496 floating-point operations (FLOPs). Additionally, this 4-layer CNN model serves as the baseline for evaluating the improvements in both performance and generalizability achieved through knowledge distillation.

The baseline model achieves an average validation accuracy of 99.69%, while the average test accuracy is 83.41%. The feature visualization of the best model on the test set is shown in Fig. 7a. The drop in accuracy clearly demonstrates the limitation of generalizability of the baseline model.

To ensure a strong baseline for knowledge distillation, we employed the Resnet model, which is widely used for this task in the relevant research [27]–[29], as the teacher model. We further evaluated Resnet models with varying structures and depths on the dataset, and the results are presented in Table IV. Considering our goal of improving both the performance and generalizability of the student model through knowledge distillation, we selected the Resnet-34 model as the teacher

TABLE IV  
EVALUATION RESULTS OF THE RESNET MODELS

Model	Val/%	Test/%	FLOPs	Params
Resnet-18	99.58	95.47	98472960	2777283
Resnet-34	99.50	97.67	226235392	8164803
Resnet-101	98.34	85.87	857427968	27532227
Resnet-152	99.07	83.04	552325120	43175875

model. The knowledge distillation process introduces two additional hyper-parameters, namely  $\alpha$  and  $T$ . To find the best combination, we iterate through different values of  $\alpha$  from 0 to 1 with a step of 0.1, and  $T$  from 1 to 10 with a step of 1. The optimal combination is found to be  $\alpha = 0.1$  and  $T = 5$ .

Through knowledge distillation, the model achieves an average test accuracy of 95.39%, while maintaining an average validation accuracy of 99.61%. The feature visualization on the test set is shown in Fig. 7b, to better demonstrate the impact of knowledge distillation. It is clear that the model trained with knowledge distillation exhibits a more distinct boundary between samples belonging to different categories, demonstrating an improvement generalizability compared with the baseline model. The comparison of the baseline model, teacher model, and student model is presented in Fig. 8. According to the figure, it is evident that the baseline model, which has fewer capacity and depth compared to the teacher model, exhibits limitations in terms of generalizability. The baseline model fails to extract high-level features that are less influenced by the training dataset, resulting in poor and unstable performance on the test dataset. It also shows that the knowledge distillation technique enables a lightweight CNN model, with only 30771 parameters and requiring 2282496 FLOPs, to achieve generalizability comparable to a larger model with 8164803 parameters and 226235392 FLOPs.

### B. Implementation Evaluation

We conduct a performance evaluation of the proposed quantization method on the resulting KD-improved models. The entire model is quantized together, meaning that all weights are quantized to the same number of shift parameters. During the quantization process, we iterate through different values of the number of shift parameters, ranging from 1 to 10. This enables us to assess and analyze the performance of the model across different degrees of quantization, thus allowing us to identify the optimal balance between compression level and performance degradation. The results of the quantization process are presented in Fig. 9a, which shows the performance of the quantized models on the validation set. Based on the results, it can be determined that the optimal number of shift parameters to be used is 3. This allows the compressed model to achieve the same performance as the original model. To validate the generalizability of the model, the quantization process is further assessed on the test dataset, as demonstrated in Fig. 9b. The results clearly indicate that the compressed model performs comparably to the original model, without any noticeable degradation in generalizability. This choice of quantization configuration effectively preserves

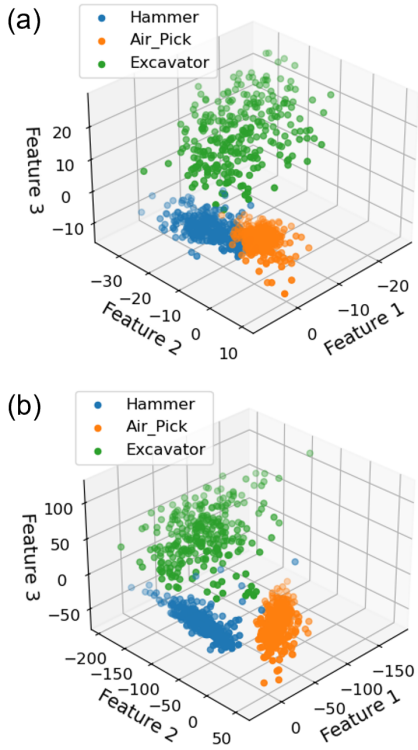


Fig. 7. Feature visualization of the models. (a) Baseline Model. (b) Improved Model.

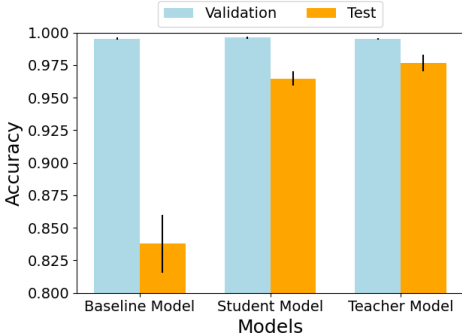


Fig. 8. Validation accuracy and test accuracy of the models.

all the essential information of the model while achieving the desired performance on the test dataset.

The encoding process is then performed to optimize the on-chip storage. It is carried out on a layer-wise basis, which means that the parameters of the same layer are encoded together using the same bias. To determine the optimal number of bits used for encoding, we conduct iterations ranging from 1 to 8. The results obtained from the validation dataset, as depicted in Fig. 10a, indicate that employing a 3-bit encoding scheme achieves lossless compression. Furthermore, the encoding process is performed on the test dataset and visualized in Fig. 10b. It is evident that the encoding procedure brings a certain degree of performance degradation in terms of the generalizability of the model. Nevertheless, despite this influence, it is worth noting that the impact remains stable and minimal. Such stability in performance degradation implies

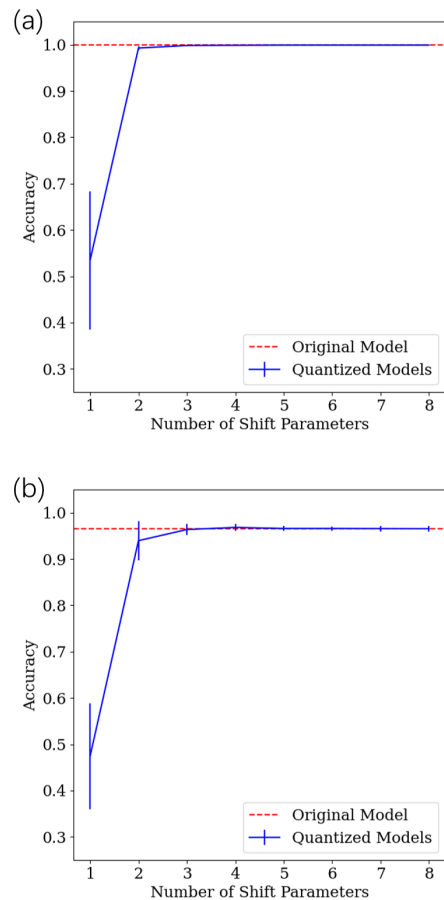


Fig. 9. Change in accuracy with number of shift parameters: (a) Accuracy change on the validation set; (b) Accuracy change on the test set.

TABLE V  
PERFORMANCE OF THE MODELS ON DIFFERENT HARDWARE

Model	Inference time on CPU/ms	Inference time on GPU/ms	Inference time on FPGA/ms
ResNet-34	1.846	0.375	-
Quantized CNN	0.254	0.178	0.083

that the encoding process does not significantly influence the overall performance of the model.

It is clear that the proposed approach offers an effective solution for achieving compression, with only a minimal impact on the generalizability of the model, as shown by the aforementioned results. We can then calculate the compression rate using the following information: the model initially consists of 30771 32-bit floating-point format parameters, and each weight is compressed into three 3-bit shift parameters. Consequently, the compression rate can be calculated:  $3 \times 3 / 32 \times 100\% = 28.125\%$ . Additionally, the proposed compression scheme has been adapted to the shift-add structure, further enhancing the overall system performance.

The optimized model is then implemented with proposed FPGA-based hardware acceleration scheme. To evaluate the proposed scheme, we use the state-of-the-art CPU and GPU as the baseline performance. Here, the utilized CPU is Intel i9-14900, GPU is Nvidia GTX 4090. The average inference

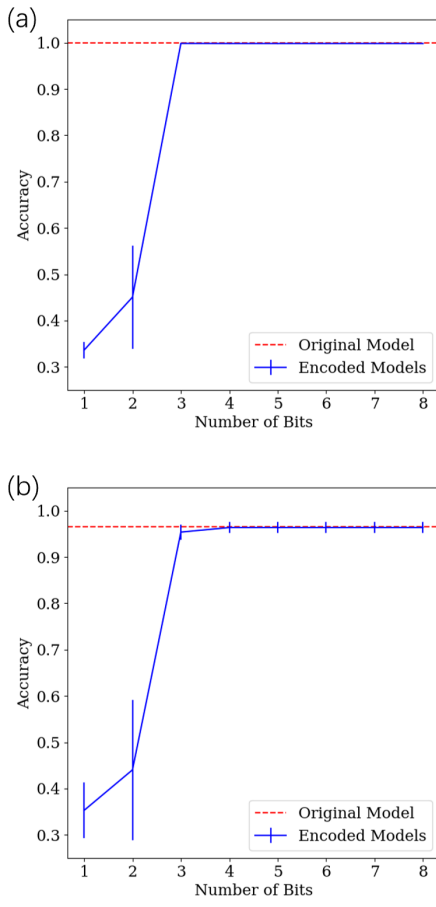


Fig. 10. Change in accuracy with number of bits used for encoding: (a) Accuracy change on the validation set. (b) Accuracy change on the test set.

time of them is shown in Table V. The FPGA chip utilized here is Xilinx ZCU15eg. For quick development and fast implementation, the design is built with Xilinx high level HLS. The final design achieved a latency of 25112 cycles running at a frequency of 303 MHz. The inference time of the system can be calculated as  $25112 \times 1/(303 \times 106) \approx 0.083ms$ . The sample time for each data frame is 256 ms, allowing the system to process 3,084 frames within this interval. This processing capacity is equivalent to handling the data generated when the system monitors a fiber with a length of  $12.5 \times 3084 = 38550m$ . Therefore, the system can achieve real-time processing over a 38-km fiber, which is longer than the 30-km fiber utilized for sampling the dataset. Based on bibliographical research, the achieved recognition time of 0.083 ms is the fastest reported so far in the field [2], [7].

TABLE VI  
HARDWARE RESOURCE UTILIZED

Resource	Utilization	Available
LUT	280828	341280
FF	257011	682560
DSP	0	3528
BRAM	11	744
URAM	0	112

The resource requirement of the design is shown in Table

VI. Our design makes efficient use of on-chip resources like look-up tables (LUT) and flip-flops (FF), allowing for high parallelism without being limited by the amount of DSP resources available. This optimization enables our system to achieve a higher performance compared with the CPU and GPU solutions.

#### IV. CONCLUSION

This paper addresses the throughput limitation issue faced by the DVS systems based on DLMs, which prevents the implementation of real-time recognition over long-distance fibers. To overcome this challenge, we propose to use lightweight models as a replacement for DLMs to reduce the computation resource requirements of the system. We identify the problem of limited generalizability of the lightweight models and adopts knowledge distillation techniques to enhance the generalizability of the utilized lightweight model. Furthermore, we propose an FPGA-based hardware acceleration scheme for fast inference. It results in an impressive 2.14x shorter inference time compared to the state-of-the-art GPU implementation, and 4.52x compared to the CPU implementation, which is also the fastest recognition time reported so far in this field. Through our proposed method, we achieve real-time recognition over 38-km-long fibers. The implemented system allows for real-time recognition over long-distance fibers in practical applications, contributing to the advancement of DVS technology and its use as a smart sensing system in various areas.

#### REFERENCES

- [1] J. Yang, C. Wang, J. Yi, Y. Du, M. Sun, S. Huang, W. Zhao, S. Qu, J. Ni, X. Xu, and Y. Shang, "Railway Intrusion Events Classification and Location Based on Deep Learning in Distributed Vibration Sensing," *Symmetry*, vol. 14, p. 2552, Dec. 2022.
- [2] N. Yang, Y. Zhao, and J. Chen, "Real-Time  $\Phi$ -OTDR Vibration Event Recognition Based on Image Target Detection," *Sensors*, vol. 22, p. 1127, Feb. 2022.
- [3] C. Lyu, Z. Huo, X. Cheng, J. Jiang, A. Alimasi, and H. Liu, "Distributed Optical Fiber Sensing Intrusion Pattern Recognition Based on GAF and CNN," *Journal of Lightwave Technology*, vol. 38, pp. 4174–4182, Aug. 2020.
- [4] X. Huang, B. Wang, K. Liu, and T. Liu, "An event recognition scheme aiming to improve both accuracy and efficiency in optical fiber perimeter security system," *Journal of Lightwave Technology*, vol. 38, pp. 5783–5790, 2020.
- [5] Y. Yang, Y. Li, T. Zhang, Y. Zhou, and H. Zhang, "Early Safety Warnings for Long-Distance Pipelines: A Distributed Optical Fiber Sensor Machine Learning Approach,"
- [6] C. Zhu, Y. Pu, K. Yang, Q. Yang, and C. L. P. Chen, "Distributed Optical Fiber Intrusion Detection by Image Encoding and SwinT in Multi-Interference Environment of Long-Distance Pipeline," *IEEE Transactions on Instrumentation and Measurement*, vol. 72, pp. 1–12, 2023.
- [7] H. Wu, Y. Wang, X. Liu, Y. Sun, G. Yan, Y. Wu, and Y. Rao, "Smart fiber-optic distributed acoustic sensing (sdas) with multitask learning for time-efficient ground listening applications," *IEEE Internet of Things Journal*, vol. 11, pp. 8511–8525, 2024.
- [8] C. Xu, J. Guan, M. Bao, J. Lu, and W. Ye, "Pattern recognition based on enhanced multifeature parameters for vibration events in  $\varphi$ -OTDR distributed optical fiber sensing system," *Microwave and Optical Technology Letters*, vol. 59, pp. 3134–3141, Dec. 2017.
- [9] H. Wu, Y. Qian, W. Zhang, and C. Tang, "Feature extraction and identification in distributed optical-fiber vibration sensing system for oil pipeline safety monitoring," *Photonic Sensors*, vol. 7, pp. 305–310, Dec. 2017.

- [10] H. Wu, X. Liu, Y. Xiao, and Y. Rao, "A Dynamic Time Sequence Recognition and Knowledge Mining Method Based on the Hidden Markov Models (HMMs) for Pipeline Safety Monitoring With  $\Phi$ -OTDR," *Journal of Lightwave Technology*, vol. 37, pp. 4991–5000, Oct. 2019.
- [11] C. Cao, X. Fan, Q. Liu, and Z. He, "Practical Pattern Recognition System for Distributed Optical Fiber Intrusion Monitoring System Based on Phase-Sensitive Coherent OTDR," in *Asia Communications and Photonics Conference 2015*, (Hong Kong), p. ASu2A.145, OSA, 2015.
- [12] X. Wang, Y. Liu, S. Liang, W. Zhang, and S. Lou, "Event identification based on random forest classifier for  $\Phi$ -OTDR fiber-optic distributed disturbance sensor," *Infrared Physics & Technology*, vol. 97, pp. 319–325, Mar. 2019.
- [13] H. Jia, S. Liang, S. Lou, and X. Sheng, "A  $\$k\$$  -Nearest Neighbor Algorithm-Based Near Category Support Vector Machine Method for Event Identification of  $\$\\varphi\$$  -OTDR," *IEEE Sensors Journal*, vol. 19, pp. 3683–3689, May 2019.
- [14] Z. Sha, H. Feng, X. Rui, and Z. Zeng, "PIG Tracking Utilizing Fiber Optic Distributed Vibration Sensor and YOLO," *JOURNAL OF LIGHTWAVE TECHNOLOGY*, vol. 39, no. 13, 2021.
- [15] W. Xu, F. Yu, S. Liu, D. Xiao, J. Hu, F. Zhao, W. Lin, G. Wang, X. Shen, W. Wang, F. Wang, H. Liu, P. P. Shum, and L. Shao, "Real-Time Multi-Class Disturbance Detection for  $\Phi$ -OTDR Based on YOLO Algorithm," *Sensors*, vol. 22, p. 1994, Mar. 2022.
- [16] X. Jin, K. Liu, J. Jiang, T. Xu, Z. Ding, X. Hu, Y. Huang, D. Zhang, S. Li, K. Xue, and T. Liu, "Pattern Recognition of Distributed Optical Fiber Vibration Sensors Based on Resnet 152," *IEEE Sensors Journal*, vol. 23, pp. 19717–19725, Sept. 2023.
- [17] W. Xu, F. Yu, S. Liu, D. Xiao, J. Hu, F. Zhao, W. Lin, G. Wang, X. Shen, W. Wang, F. Wang, H. Liu, P. P. Shum, and L. Shao, "Real-time multi-class disturbance detection for  $\phi$ -otdr based on yolo algorithm," *Sensors (Basel, Switzerland)*, vol. 22, 2022.
- [18] J. Meng, S. K. Venkataramanaiyah, C. Zhou, P. Hansen, P. N. Whatmough, and J. sun Seo, "Fixyfpga: Efficient fpga accelerator for deep neural networks with high element-wise sparsity and without external memory access," *2021 31st International Conference on Field-Programmable Logic and Applications (FPL)*, pp. 9–16, 2021.
- [19] G. Hinton, O. Vinyals, and J. Dean, "Distilling the Knowledge in a Neural Network," Mar. 2015.
- [20] H.-J. Kang, "Aocstream: All-on-chip cnn accelerator with stream-based line-buffer architecture," *Proceedings of the 2023 ACM/SIGDA International Symposium on Field Programmable Gate Arrays*, 2022.
- [21] T. K. Arrestad, V. Loncar, N. Ghielmetti, M. Pierini, S. P. Summers, J. Ngadiuba, C. Petersson, H. Linander, Y. Iiyama, G. D. Guglielmo, J. M. Duarte, P. C. Harris, D. S. Rankin, S. Jindariani, K. Pedro, N. V. Tran, M. Liu, E. Kreinar, Z. Wu, and D. Hoang, "Fast convolutional neural networks on fpgas with hls4ml," *Machine Learning: Science and Technology*, vol. 2, 2021.
- [22] A. Anupreetham, M. Ibrahim, M. Hall, A. Boutros, A. Kuzhively, A. Mohanty, E. Nurvitadhi, V. Betz, Y. Cao, and J. sun Seo, "End-to-end fpga-based object detection using pipelined cnn and non-maximum suppression," *2021 31st International Conference on Field-Programmable Logic and Applications (FPL)*, pp. 76–82, 2021.
- [23] W. Pang, C. Wu, and S. Lu, "An energy-efficient implementation of group pruned cnns on fpga," *IEEE Access*, vol. 8, pp. 217033–217044, 2020.
- [24] V. Sze, Y.-H. Chen, T.-J. Yang, and J. S. Emer, "Efficient processing of deep neural networks: A tutorial and survey," *Proceedings of the IEEE*, vol. 105, no. 12, pp. 2295–2329, 2017.
- [25] A. Gholami, S. Kim, Z. Dong, Z. Yao, M. W. Mahoney, and K. Keutzer, "A survey of quantization methods for efficient neural network inference," *ArXiv*, vol. abs/2103.13630, 2021.
- [26] M. Todd, "2 - sensor data acquisition systems and architectures," in *Sensor Technologies for Civil Infrastructures* (M. Wang, J. Lynch, and H. Sohn, eds.), vol. 55 of *Woodhead Publishing Series in Electronic and Optical Materials*, pp. 23–56, Woodhead Publishing, 2014.
- [27] Z. Ge, H. Wu, C. Zhao, and M. Tang, "High-accuracy event classification of distributed optical fiber vibration sensing based on time–space analysis," *Sensors (Basel, Switzerland)*, vol. 22, 2022.
- [28] X. Jin, K. Liu, J. Jiang, T. Xu, Z. Ding, X. Hu, Y. Huang, D. Zhang, S. Li, K. Xue, and T. Liu, "Pattern recognition of distributed optical fiber vibration sensors based on resnet 152," *IEEE Sensors Journal*, vol. 23, pp. 19717–19725, 2023.
- [29] R. Yao, J. Li, J. Zhang, and Y. Wei, "Vibration event recognition using sst-based  $\phi$ -otdr system," *Sensors (Basel, Switzerland)*, vol. 23, 2023.

**Zhongyao Luo** received his BEng degree in Electronics and Computer Science from the University of Edinburgh in 2020. He is currently working toward a PhD at the School of Optical and Electronic Information, HUST, Wuhan, China. His current research interests include distributed optical fiber sensing, and machine learning.

**Hao Wu** received his BS, MS, and PhD degrees from HUST, Wuhan, China, in 2013, 2016, and 2019, respectively. His postdoctoral research at HUST was focused on the machine learning algorithms for distributed optical fiber sensing. Since 2024, he has been a research associate at HUST. His current research interests are the integration of artificial intelligence and optical fiber.

**Zhao Ge** received his BS degree from Jianghan University, Wuhan, China, in 2019 and his MD degree from HUST, Wuhan, China, in 2022. He is currently working toward a PhD at the School of Optical and Electronic Information, HUST, Wuhan, China.

**Ming Tang** received his BEng degree from HUST in 2001 and his PhD from Nanyang Technological University, Singapore, in 2005. His postdoctoral research at the Network technology Research Center was focused on the optical fiber amplifier. From 2009, he was a research scientist in the Tera-Photonics Group, RIKEN, Japan. Since 2011, he has been a professor at HUST. His current research interests include optical fiber-based linear and nonlinear effects for communication and sensing applications.